Effect of probe beam intensity on all-optical switching based on excited-state absorption

Parag Sharma[1,2,*] and Sukhdev Roy[1,3]

[1]*Department of Physics and Computer Science, Dayalbagh Educational Institute, Agra 282 110, India*
[2]*Currently with the Quantum Optics and Photon Physics Group, CSIR-National Physical Laboratory, Dr. K.S. Krishnan Road, New Delhi 110012, India*
[3]*sukhdevroy@dei.ac.in*
**sharmap2@nplindia.org*

Abstract: We theoretically analyze the effect of probe beam intensity on all-optical switching based on nonlinear absorption, using the pump-probe configuration. To draw general inferences that are applicable to a wide range of polyatomic molecules, we consider as a typical example, switching in *pharaonis* phoborhodopsin (*p*pR) protein and its mutants that exhibit a complex photocycle similar to bacteriorhodopsin (bR), having a number of intermediates with respective absorption spectra spanning the entire visible region. The switching of the transmission of a cw probe beam by a pulsed pump beam has been studied in detail at different wavelength combinations. Interesting consequences emerge from the present analysis. It is shown that by controlling the probe intensity, the switching characteristics can be inverted, switching time can be reduced and the profile of the switched probe beam and the switching contrast can be controlled. For some cases, the switching contrast can also be maximized by optimizing the probe intensity. Increase in probe intensity also leads to increase in switching contrast under certain conditions. At particular spectral and kinetic conditions, the nonlinear optical material appears linear for a given probe intensity and pump-probe wavelengths, respectively. Variation in probe intensity thus provides an effective means to modify the switching characteristics instead of using mutants with different rate constants for a variety of nonlinear absorption based all-optical devices.

OCIS codes: (190.4400) Nonlinear optics, materials; (230.1150) All-optical devices.

References and links

1. V. R. Almeida, C. A. Barrios, R. R. Panepucci, and M. Lipson, "All-optical control of light on a silicon chip," Nature **431**(7012), 1081–1084 (2004).
2. S. A. Haque and J. Nelson, "Physics. Toward organic all-optical switching," Science **327**(5972), 1466–1467 (2010).
3. S. F. Mingaleev, A. E. Miroshnichenko, Y. S. Kivshar, and K. Busch, "All-optical switching, bistability, and slow-light transmission in photonic crystal waveguide-resonator structures," Phys. Rev. E Stat. Nonlin. Soft Matter Phys. **74**(4), 046603 (2006).
4. X. Hu, P. Jiang, C. Ding, H. Yang, and Q. Gong, "Picosecond and low-power all-optical switching based on an organic photonic bandgap microcavity," Nat. Photonics **2**(3), 185–189 (2008).
5. D. N. Christodoulides, I. C. Khoo, G. J. Salamo, G. I. Stegeman, and E. W. Van Stryland, "Nonlinear refraction and absorption: mechanisms and magnitudes," Adv. Opt. Photon. **2**(1), 60–200 (2010).
6. J. M. Hales, J. Matichak, S. Barlow, S. Ohira, K. Yesudas, J. L. Brédas, J. W. Perry, and S. R. Marder, "Design of polymethine dyes with large third-order optical nonlinearities and loss figures of merit," Science **327**(5972), 1485–1488 (2010).
7. G. A. Wurtz, R. Pollard, W. Hendren, G. P. Wiederrecht, D. J. Gosztola, V. A. Podolskiy, and A. V. Zayats, "Designed ultrafast optical nonlinearity in a plasmonic nanorod metamaterial enhanced by nonlocality," Nat. Nanotechnol. **6**(2), 107–111 (2011).
8. X. Chen, J. Tao, G. Zou, W. Su, Q. Zhang, and P. Wang, "Thermosensitive silver/polydiacetylene nanocrystals with tunable nonlinear optical properties," ChemPhysChem **11**(17), 3599–3603 (2010).
9. H. Abdeldayem, D. O. Frazier, and M. S. Paley, "An all-optical picosecond switch in polydiacetylene," Appl. Phys. Lett. **82**(7), 1120–1122 (2003).

#160815 - $15.00 USD Received 3 Jan 2012; revised 8 Mar 2012; accepted 20 Mar 2012; published 6 Apr 2012

10. C. Li, L. Zhang, M. Yang, H. Wang, and Y. Wang, "Dynamic and steady-state behaviors of reverse saturable absorption in metallophthalocyanine," Phys. Rev. A **49**(2), 1149–1157 (1994).
11. S. Roy and C. Yadav, "All-optical ultrafast logic gates based on saturable to reverse saturable absorption transition in CuPc-doped PMMA thin films," Opt. Commun. **284**(19), 4435–4440 (2011).
12. C. Li, L. Zhang, R. Wang, Y. Song, and Y. J. Wang, "Dynamics of reverse saturable absorption and all-optical switching in C_{60}," J. Opt. Soc. Am. B **11**(8), 1356–1360 (1994).
13. H. Wang, H. Su, H. Qian, Z. Wang, X. Wang, and A. Xia, "Structure-dependent all-optical switching in graphene-nanoribbon-like molecules: fully conjugated tri(perylene bisimides)," J. Phys. Chem. A **114**(34), 9130–9135 (2010).
14. R. R. Dasari, M. M. Sartin, M. Cozzuol, S. Barlow, J. W. Perry, and S. R. Marder, "Synthesis and linear and nonlinear absorption properties of dendronised ruthenium(II) phthalocyanine and naphthalocyanine," Chem. Commun. (Camb.) **47**(15), 4547–4549 (2011).
15. G. S. He, J. Zhu, A. Baev, M. Samoć, D. L. Frattarelli, N. Watanabe, A. Facchetti, H. Ågren, T. J. Marks, and P. N. Prasad, "Twisted π-system chromophores for all-optical switching," J. Am. Chem. Soc. **133**(17), 6675–6680 (2011).
16. F. Z. Henari and S. Cassidy, "Non-linear optical properties and all-optical switching of congo red in solution," Optik (Stuttg.) (to be published).
17. K. Zhang, J. Li, W. Wang, J. Xiao, W. Yin, and L. Yu, "Enhancing the linear absorption and tuning the nonlinearity of TiO_2 nanowires through the incorporation of Ag nanoparticles," Opt. Lett. **36**(17), 3443–3445 (2011).
18. P. Sharma, S. Roy, and C. P. Singh, "Dynamics of all-optical switching in polymethine dye molecules," Thin Solid Films **477**(1-2), 42–47 (2005).
19. C. P. Singh, K. S. Bindra, B. Jain, and S. M. Oak, "All-optical switching characteristics of metalloporphyrins," Opt. Commun. **245**(1-6), 407–414 (2005).
20. A. Charas, A. L. Mendonça, J. Clark, L. Bazzana, A. Nocivelli, G. Lanzani, and J. Morgado, "Stimulated emission and ultrafast optical switching in a ter(9,9′-spirobifluorene)-co-methylmethacrylate copolymer," J. Polym. Sci., B, Polym. Phys. **49**(1), 52–61 (2011).
21. M. Hari, S. Mathew, B. Nithyaja, S. A. Joseph, V. P. N. Nampoori, and P. Radhakrishnan, "Saturable and reverse saturable absorption in aqueous silver nanoparticles at off-resonant wavelngth," Opt. Quantum Electron. **43**(1-5), 49–58 (2012).
22. D. Oesterhelt, C. Bräuchle, and N. Hampp, "Bacteriorhodopsin: a biological material for information processing," Q. Rev. Biophys. **24**(4), 425–478 (1991).
23. R. R. Birge, "Protein-based optical computing and memories," IEEE Comput. **25**(11), 56–67 (1992).
24. N. Hampp, "Bacteriorhodopsin as a photochromic retinal protein for optical memories," Chem. Rev. **100**(5), 1755–1776 (2000).
25. K. J. Wise and R. R. Birge, "Biomolecular photonics based on bacteriorhodopsin," in *CRC Handbook of Organic Photochemistry and Photobiology,* 2nd ed., F. Lenci and W. Horspool, eds. (CRC Press, 2003), Vols. 1 & 2, Chap. 135.
26. K. J. Wise, N. B. Gillespie, J. A. Stuart, M. P. Krebs, and R. R. Birge, "Optimization of bacteriorhodopsin for bioelectronic devices," Trends Biotechnol. **20**(9), 387–394 (2002).
27. P. Wu, D. V. G. L. N. Rao, B. R. Kimball, M. Nakashima, and B. S. DeCristofano, "Enhancement of photoinduced anisotropy and all-optical switching in bacteriorhodopsin films," Appl. Phys. Lett. **81**(20), 3888–3890 (2002).
28. S. Roy, C. P. Singh, and K. P. J. Reddy, "Analysis of all optical switching in bacteriorhodopsin," Curr. Sci. **83**, 623–627 (2002).
29. K. P. J. Reddy, "Analysis of light-induced processes in bacteriorhodopsin and its application for spatial light modulation," J. Appl. Phys. **77**(12), 6108–6113 (1995).
30. C. P. Singh and S. Roy, "All-optical switching in bacteriorhodopsin based on M state dynamics and its application to photonic logic gates," Opt. Commun. **218**(1-3), 55–66 (2003).
31. P. Sharma, "Enhancement of speed of digital operation in bacteriorhodopsin based photonic switches," Optik (Stuttg.) **121**(4), 384–388 (2010).
32. S. Roy, P. Sharma, A. K. Dharmadhikari, and D. Mathur, "All-optical switching with bacteriorhodopsin," Opt. Commun. **237**(4-6), 251–256 (2004).
33. Y. Huang, S. T. Wu, and Y. Zhao, "All-optical switching characteristics in bacteriorhodopsin and its applications in integrated optics," Opt. Express **12**(5), 895–906 (2004).
34. R. K. Banyal and B. R. Prasad, "High-contrast, all-optical switching in bacteriorhodopsin films," Appl. Opt. **44**(26), 5497–5503 (2005).
35. J. Topolancik and F. Vollmer, "All-optical switching in the near infrared with bacteriorhodopsin-coated microcavities," Appl. Phys. Lett. **89**(18), 184103 (2006).
36. J. L. Spudich and H. Luecke, "Sensory rhodopsin II: functional insights from structure," Curr. Opin. Struct. Biol. **12**(4), 540–546 (2002).
37. R. Moukhametzianov, J. P. Klare, R. Efremov, C. Baeken, A. Göppner, J. Labahn, M. Engelhard, G. Büldt, and V. I. Gordeliy, "Development of the signal in sensory rhodopsin and its transfer to the cognate transducer," Nature **440**(7080), 115–119 (2006).
38. N. Kamo, K. Shimono, M. Iwamoto, and Y. Sudo, "Photochemistry and photoinduced proton-transfer by *pharaonis* phoborhodopsin," Biochemistry Mosc. **66**(11), 1277–1282 (2001).

#160815 - $15.00 USD Received 3 Jan 2012; revised 8 Mar 2012; accepted 20 Mar 2012; published 6 Apr 2012

39. M. Miyazaki, J. Hirayama, M. Hayakawa, and N. Kamo, "Flash photolysis study on *pharaonis* phoborhodopsin from a haloalkaliphilic bacterium (*Natronobacterium pharaonis*)," Biochim. Biophys. Acta **1140**(1), 22–29 (1992).
40. Y. Imamoto, Y. Shichida, J. Hirayama, H. Tomioka, N. Kamo, and T. Yoshizawa, "Nanosecond laser photolysis of phoborhodopsin: from *natronobacterium pharaonis* appearance of KL and L intermediates in the photocycle at room temperature," Photochem. Photobiol. **56**(6), 1129–1134 (1992).
41. P. Sharma, "Fast photonic switching in *pharaonis* phoborhodopsin protein molecules," J. Biophotonics **1**(6), 526–530 (2008).
42. P. Sharma and S. Roy, "All-optical light modulation in *pharaonis* phoborhodopsin and its application to parallel logic gates," J. Appl. Phys. **96**(3), 1687–1695 (2004).
43. P. Sharma, S. Roy, and C. P. Singh, "Low power spatial light modulator with *pharaonis* phoborhodopsin," Thin Solid Films **477**(1-2), 227–232 (2005).
44. S. Roy, T. Kikukawa, P. Sharma, and N. Kamo, "All-optical switching in *Pharaonis* phoborhodopsin protein molecules," IEEE Trans. Nanobioscience **5**(3), 178–187 (2006).
45. M. Iwamoto, K. Shimono, M. Sumi, and N. Kamo, "Positioning proton-donating residues to the Schiff-base accelerates the M-decay of *pharaonis* phoborhodopsin expressed in *Escherichia coli*," Biophys. Chem. **79**(3), 187–192 (1999).
46. K. Takao, T. Kikukawa, T. Araiso, and N. Kamo, "Azide accelerates the decay of M-intermediate of *pharaonis phoborhodopsin*," Biophys. Chem. **73**(1-2), 145–153 (1998).
47. Y. Sudo, M. Iwamoto, K. Shimono, and N. Kamo, "Association of *pharaonis* phoborhodopsin with its cognate transducer decreases the photo-dependent reactivity by water-soluble reagents of azide and hydroxylamine," Biochim. Biophys. Acta **1558**(1), 63–69 (2002).
48. K. Shimono, M. Iwamoto, M. Sumi, and N. Kamo, "V108M mutant of *pharaonis* phoborhodopsin: substitution caused no absorption change but affected its M-state," J. Biochem. **124**(2), 404–409 (1998).
49. M. Iwamoto, Y. Sudo, K. Shimono, T. Araiso, and N. Kamo, "Correlation of the O-intermediate rate with the pKa of Asp-75 in the dark, the counterion of the Schiff base of *pharaonis* phoborhodopsin (sensory rhodopsin II)," Biophys. J. **88**(2), 1215–1223 (2005).
50. C. P. Singh and S. Roy, "Analysis of low power spatial light modulation characteristics of bacteriorhodopsin," Optik (Stuttg.) **113**(9), 373–381 (2002).
51. Z. Bálint, M. Lakatos, C. Ganea, J. K. Lanyi, and G. Váró, "The nitrate transporting photochemical reaction cycle of the pharaonis halorhodopsin," Biophys. J. **86**(3), 1655–1663 (2004).
52. S. Roy and P. Sharma, "Analysis of all-optical light modulation in proteorhodopsin protein molecules," Optik (Stuttg.) **119**(4), 192–202 (2008).
53. L. Ujj, S. Devanathan, T. E. Meyer, M. A. Cusanovich, G. Tollin, and G. H. Atkinson, "New photocycle intermediates in the photoactive yellow protein from *Ectothiorhodospira halophila*: picosecond transient absorption spectroscopy," Biophys. J. **75**(1), 406–412 (1998).
54. S. Roy and K. Kulshrestha, "All-optical switching in plant blue light photoreceptor phototropin," IEEE Trans. Nanobioscience **5**(4), 281–287 (2006).
55. Y. Shen, C. R. Safinya, K. S. Liang, A. F. Ruppert, and J. Rothschild, "Stabilization of the membrane protein bacteriorhodopsin to 140°C in two-dimensional films," Nature **366**(6450), 48–50 (1993).
56. E. P. Lukashev and B. Robertson, "Bacteriorhodopsin retains its light-induced proton-pumping function after being heated to 140°C," Bioelectrochem. Bioenerg. **37**(2), 157–160 (1995).
57. Y. Sudo, M. Yamabi, M. Iwamoto, K. Shimono, and N. Kamo, "Interaction of *Natronobacterium pharaonis* phoborhodopsin (sensory rhodopsin II) with its cognate transducer probed by increase in the thermal stability," Photochem. Photobiol. **78**(5), 511–516 (2003).
58. S. Schenkl, F. van Mourik, N. Friedman, M. Sheves, R. Schlesinger, S. Haacke, and M. Chergui, "Insights into excited-state and isomerization dynamics of bacteriorhodopsin from ultrafast transient UV absorption," Proc. Natl. Acad. Sci. U.S.A. **103**(11), 4101–4106 (2006).
59. S. Roy, M. Prasad, J. Topolancik, and F. Vollmer, "All-optical switching with bacteriorhodopsin protein coated microcavities and its application to low-power computing circuits," J. Appl. Phys. **107**(5), 053115 (2010).
60. S. Roy, P. Sethi, J. Topolancik, and F. Vollmer, "All-optical reversible logic gates with bacteriorhodopsin protein coated microresonators," Adv. Opt. Technol. **2012**, 727206 (2012).
61. P. Wu and D. V. G. L. N. Rao, "Controllable snail-paced light in biological bacteriorhodopsin thin film," Phys. Rev. Lett. **95**(25), 253601 (2005).

1. Introduction

Switching light with light is of tremendous importance for both fundamental and applied science [1–4]. A switch is the basic building block of information processing systems. The advent of nano-photonics has led to the design, synthesis and characterization of novel molecules that exhibit an efficient nonlinear optical response, which can be utilized for designing molecular all-optical switches [5–8]. In addition to advantages of small size and weight, high intrinsic speed, extremely low propagation delay and power dissipation, the properties can be tailored by physical, chemical and genetic engineering techniques to suit desired applications [5–8].

#160815 - $15.00 USD Received 3 Jan 2012; revised 8 Mar 2012; accepted 20 Mar 2012; published 6 Apr 2012

A promising mechanism for all-optical switching is the phenomenon of excited-state absorption (ESA), in which a pump beam excites the molecules from the ground to the excited-state that leads to switching of the transmission of a probe beam. All-optical switching based on ESA, using a pump-probe configuration, is a simple, flexible and convenient technique for practical applications, compared to other methods, for instance, those based on phase conjugation and interference phenomena [9–21]. The transmission of the cw probe beam gets modulated due to the intensity-induced changes in the population of the ground and excited states by a cw or pulsed pump beam depending on the kinetic and spectral response of the material [18–20]. All-optical switching based on ESA, using the pump-probe technique, has been recently reported in a variety of organic and inorganic systems that include, polydiacetylene [9], metallophthalocyanine [10,11], C_{60} [12], graphene [13], organometallic phthalocyanine [14], twisted π-system chromophores [15], congo red solution [16], TiO_2 nanowires [17], polymethine dyes [18], metalloporphyrins [19], and Ter(9,9′-spirobifluorene)-co-methylmethacrylate cpolymer [20] and aqueous silver nanoparticles [21].

In general, as in transient absorption spectroscopy, the intensity of the probe beam is considered to be very weak compared to the pump beam so that the probe beam does not affect the material response. The switching characteristics are not affected by the probe beam intensity, provided the absorption spectra of the ground and the excited-state do not overlap each other. However, usually, the absorption spectra of the excited-states overlap and hence, the probe beam gets absorbed by the ground state also, which can affect the switching characteristics. Moreover, practical implementation of digital logic devices based on the pump-probe configuration would require cascading, which can be possible if we consider the intensity of the probe beam to be of the order of the pump beam intensity or more. In addition to this, in case of nonlinear absorbers such as photosensitive proteins that exhibit a complex photocycle, with a number of intermediates having respective absorption spectra, the switching characteristics can be controlled by varying the probe beam intensity at a suitable wavelength. In such cases, the switching contrast, time, profile and relative phase between the pump and the switched probe beam would be affected by the probe beam intensity. Hence, a detailed study of the effect of probe beam intensity on switching characteristics is important that can lead to interesting consequences.

It would be appropriate to consider a photochromic material that exhibits a complex photoresponse, from which general inferences can be drawn. Of the wide variety of materials studied for all-optical switching, naturally occurring photosensitive biomolecules optimized over centuries of evolution, whose spectral and kinetic properties can be tailored through physical, chemical and genetic engineering, appear to be quite fascinating. The large family of rhodopsin proteins exhibits an efficient photoresponse, with the photochromic Bacteriorhodopsin (bR) protein found in the purple membrane of *Halobacterium halobium* having attracted most attention for bio-molecular photonic applications [22–35]. Recently, a new blue-shifted photoreceptor sensory rhodopsin II (sRII) or phoborhodopsin (pR) like protein, synthesized from *Natronobacterium pharaonis*, a halophilic alkaliphilic bacterium termed *pharaonis* phoborhodopsin (*p*pR), has received much attention due to its good stability and recent structure elucidation [36–38]. The excitation of bR or *p*pR molecules by 570 nm or 498 nm light, respectively, induces a photocycle, in which, the excited molecule undergoes several conformational changes, forming a number of intermediate states, before finally relaxing back to their respective initial states [24,25,28–44].

The typical photocycle of WT-*p*pR is shown in Fig. 1 [38–43]. After excitation with 498 nm wavelength light, the molecule gets excited from the initial *p*pR state to the K-state and transforms to the KL-state within 50 ns. From there, it transforms in 990 ns into the L-state. From the L-state, the molecules transform to the M-state in about 32 μs. The species in the M-state relax to the O intermediate state in 1.7 s, from which it finally relaxes to the initial *p*pR state in 770 ms. The intermediates are named in analogy to those in the photocycle of bR. The different intermediate states exhibit respective absorption spectra spanning the entire visible region [39,40]. Any intermediate state within the photocycle can be switched directly to the initial state by shining light corresponding to its peak absorption wavelength [28–40]. Hence,

#160815 - $15.00 USD Received 3 Jan 2012; revised 8 Mar 2012; accepted 20 Mar 2012; published 6 Apr 2012

controlling the population dynamics by probe beam intensity at different wavelengths provides a great deal of flexibility for device applications.

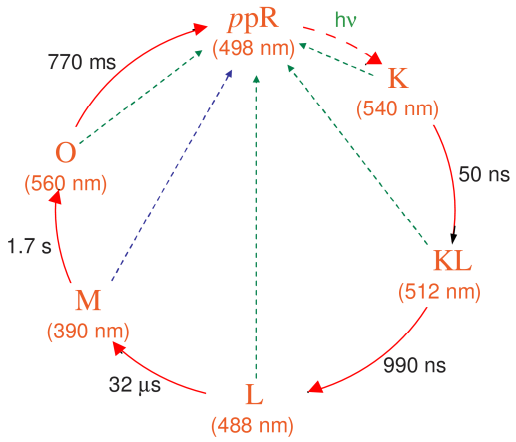

Fig. 1. Schematic of the typical photocycle of *p*pR molecule. The maximum absorption wavelengths of the intermediates are shown in brackets. Solid and dashed arrows represent thermal and photo-induced transitions respectively.

The rate constants and absorption spectra of *p*pR intermediate states can be altered through various physical, chemical and biotechnological procedures, such as variation in the polymer environment, including pH, temperature and degree of hydration and addition of chemicals [45–49]. For instance, addition of azide affects the absorption spectra and the M-state lifetime [46,47], and replacing the amino acid (Val-108) by methionine (V108M mutant of *p*pR) causes three times faster decay of M-state and removes the shoulder of the M-state spectrum [39]. Various mutants of *p*pR at different pH values having different values of rate constants of M and O intermediate states have been reported recently [45,49].

All-optical switching in bR and *p*pR, and their mutants, based on ESA, has been extensively studied theoretically and experimentally in the pump-probe geometry using cw and pulsed pump beams [27–34,41–44]. In most of the studies, the probe beam is considered to be very weak in comparison to the pump beam [28–30,41–43]. The switching characteristics have been used to design spatial light modulators (SLMs) and logic gates that are integral components of all-optical computing systems [29,30,33,41–43]. The *p*pR photocycle exhibits longer lifetimes of the M and O intermediate states in comparison to corresponding states of bR even in its native state i.e. the wild-type (WT) form, and hence leads to all-optical switching at considerably lower pump power in comparison to bR [28–30,38–44].

Recently, we have presented an improved theoretical model that incorporates the effect of probe intensity on all-optical switching characteristics of bR and *p*pR [32,44]. The effect of pump beam intensity, pump pulse width, pump pulse frequency and pump pulse profile has been studied on switching characteristics. The theoretical results have been shown to be in good agreement with experimental results [32,44]. Huang *et al.* have observed flipping of the phase of the switched probe beam with change in its intensity in bR [33]. We have also conducted preliminary experimental and theoretical simulations of switching in *p*pR that show that increasing the probe intensity leads to continuous change in the apparent phase shift between the pump and probe beams [44].

The detailed analysis of the effect of probe beam intensity on switching characteristics of bR or *p*pR would provide a means to control its various features. In addition, it would also provide a general understanding applicable to a large number of photosensitive proteins and other molecules that exhibit partially some form of its photo-response. Hence, the aim of this paper is (i) to theoretically analyze the effect of probe beam intensity on all-optical switching characteristics of WT-*p*pR protein and its mutants based on ESA, especially, on switching

#160815 - $15.00 USD Received 3 Jan 2012; revised 8 Mar 2012; accepted 20 Mar 2012; published 6 Apr 2012

contrast, switching time and switched probe beam profile, (ii) to determine the condition for maximum switching contrast, and (iii) to draw general inferences for the effect of probe beam intensity that are applicable to other materials.

2. Theoretical model

We consider all-optical switching based on ESA using the pump-probe technique. A pulsed pump beam excites the molecules to populate the intermediates that absorb a cw probe beam depending on the absorption spectra and the probe transmission gets switched [28–30,32–34,41–44]. Mathematically, the nonlinear interaction is described with population densities of the matter states and the intensities of the light fields.

We consider the typical photocycle of *p*pR as shown in Fig. 1 [39–43]. To simulate the effect of the intensity of both the pump and probe beams, we consider *p*pR molecules exposed to light beams of intensities I_m' and I_p', which modulate the population densities of different states through the excitation and de-excitation processes and can be described by the rate equations in the following form

$$\begin{aligned}
\frac{dN_R(t)}{dt} &= -\left(I_m\sigma_R\psi_R + I_p\sigma_{Rp}\right)N_R(t) + \left(I_m\sigma_K + I_p\sigma_{Kp}\right)N_K(t) + \left(I_m\sigma_{KL} + I_p\sigma_{KLp}\right)N_{KL}(t) \\
&\quad + \left(I_m\sigma_L + I_p\sigma_{Lp}\right)N_L(t) + \left(I_m\sigma_M + I_p\sigma_{Mp}\right)N_M(t) + \left(k_O + I_m\sigma_O + I_p\sigma_{Op}\right)N_O(t) \\
\frac{dN_K(t)}{dt} &= \left(I_m\sigma_R\psi_R + I_p\sigma_{Rp}\right)N_R(t) - \left(k_K + I_m\sigma_K + I_p\sigma_{Kp}\right)N_K(t) \\
\frac{dN_{KL}(t)}{dt} &= k_K N_K(t) - \left(k_{KL} + I_m\sigma_{KL} + I_p\sigma_{KLp}\right)N_{KL}(t) \\
\frac{dN_L(t)}{dt} &= k_{KL}N_{KL}(t) - \left(k_L + I_m\sigma_L + I_p\sigma_{Lp}\right)N_L(t) \\
\frac{dN_M(t)}{dt} &= k_L N_L(t) - \left(k_M + I_m\sigma_M + I_p\sigma_{Mp}\right)N_M(t) \\
\frac{dN_O(t)}{dt} &= k_M N_M(t) - \left(k_O + I_m\sigma_O + I_p\sigma_{Op}\right)N_O(t)
\end{aligned} \tag{1}$$

where N_i, $i = R, K, KL, L, M$ and O are the population densities of *p*pR, K, KL, L, M and O states, respectively; σ_i and k_i are the absorption cross-sections and rate constants of respective states, subscript p denotes the value at probe wavelength; $\psi_R = 0.51$ is the quantum efficiency for the *p*pR→K transition [38]. I_m and I_p are the photon density flux of the pump laser beam and probe laser beam, respectively. The typical numerical values of rate constants and absorption cross-sections for various intermediates in the typical *p*pR photocycle at different wavelengths are given in Table 1 [39–43].

We consider a Gaussian pump laser pulse given by

$$I_m' = I_{m0}'\left(-c\left(\frac{t-t_m}{\Delta t}\right)^2\right) \tag{2}$$

where I_{mo}' is the peak pump intensity, t_m is the time at which the respective pulse maxima occur, $c = 4\ln 2$ is the pulse profile parameter and Δt is the pulse width [28–30].

We consider the transmission of a cw probe laser beam of intensity I_p', modulated by absorption due to different states that get populated due to excitation of *p*pR molecules by both the pulsed pump laser beam and a cw probe beam. The nonlinear intensity-dependent absorption coefficient for the probe beam is written as [32]

#160815 - $15.00 USD Received 3 Jan 2012; revised 8 Mar 2012; accepted 20 Mar 2012; published 6 Apr 2012

$$\alpha_p\left(I_m, I_p\right) = N_R\left(I_m, I_p\right)\sigma_{Rp} + N_K\left(I_m, I_p\right)\sigma_{Kp} + N_{KL}\left(I_m, I_p\right)\sigma_{KLp} + N_L\left(I_m, I_p\right)\sigma_{Lp} + N_M\left(I_m, I_p\right)\sigma_{Mp} + N_O\left(I_m, I_p\right)\sigma_{Op} \quad (3)$$

As our earlier experimental and theoretical results with *p*pR are in good agreement considering the thin sample approximation, the normalized transmitted probe intensity (NTPI) is given by a simplified equation [44]

$$\frac{I_{pout}}{I_{pin}} = \exp\{-\alpha_p\left(I_m, I_p\right)L\} \quad (4)$$

where L is the thickness of the medium.

Table 1. Absorption Cross-sections and Rate Constants of Different Intermediates of WT-*p*pR [39–44]

Rate Constant	WT-*p*pR Value (s^{-1})	Absorption Cross-Section	Value (cm^2)		
			498 nm	390 nm	560 nm
		σ_R	1.6×10^{-16}	3.2×10^{-17}	1.6×10^{-17}
k_K	2.0×10^7	σ_K	6.4×10^{-17}	0	0
k_{KL}	1.0×10^6	σ_{KL}	1.3×10^{-16}	3.2×10^{-17}	4.3×10^{-17}
k_L	3.1×10^4	σ_L	1.0×10^{-16}	3.2×10^{-17}	1.6×10^{-17}
k_M	0.59	σ_M	0	1.5×10^{-16}	0
k_O	1.3	σ_O	4.4×10^{-17}	0	1.76×10^{-16}

3. Results and discussion

The all-optical switching characteristics namely the variation in the NTPI with time have been computed using Eqs. (1)–(4), with peak pump intensity $I_{m0}' = 50$ mW/cm^2, sample thickness $L = 5$ mm and pump pulse width $\Delta t = 1$ s. The typical values of the rate constants and absorption cross-sections of various states are given in Table 1 [39–44]. To study the effect of a strong probe beam in addition to the pump beam at different spectral and kinetic conditions, we consider switching in native wild-type *p*pR and its two mutants that exhibit considerable change in rate constants of their intermediates while retaining the same absorption spectra, i.e., (i) WT-*p*pR ($k_M = 0.59$ s^{-1}, $k_O = 1.3$ s^{-1}), (ii) F86D/L40T-*p*pR ($k_M = 190$ s^{-1}, $k_O = 0.66$ s^{-1}) and (iii) F86D-*p*pR ($k_M = 11$ s^{-1}, $k_O = 0.83$ s^{-1}) [45]. We consider various cases of all-optical switching with different pump-probe combinations to analyse switching at peak absorption wavelength of the longer lifetime M and O intermediates.

3.1 Wild-Type ppR

The M-intermediate state has the longest lifetime in WT-*p*pR and doesn't show absorption at the peak absorption wavelength of other intermediate states [39–44]. Figure 2(a) shows the variation in the NTPI at 390 nm, corresponding to the peak absorption of M-intermediate state, with time, for different I_p' values, with concentration of 47.02 μM and $I_{m0}' = 50$ mW/cm^2. The concentration considered is at the optimum value for maximum switching contrast considering a weak probe beam [18]. Interestingly, as I_p' increases, switching time decreases along with the switching contrast. The profile of switched probe beam becomes more symmetric with increase in I_p'. As is well known, for a weak probe beam, for γ (ratio of probed to ground state absorption cross-section at probe wavelength) >1, the NTPI switches low as the pump pulse excites the sample (Fig. 2(a)), due to absorption of the probe by molecules in the *p*pR$_M$ state, Fig. 2(b).

#160815 - $15.00 USD Received 3 Jan 2012; revised 8 Mar 2012; accepted 20 Mar 2012; published 6 Apr 2012

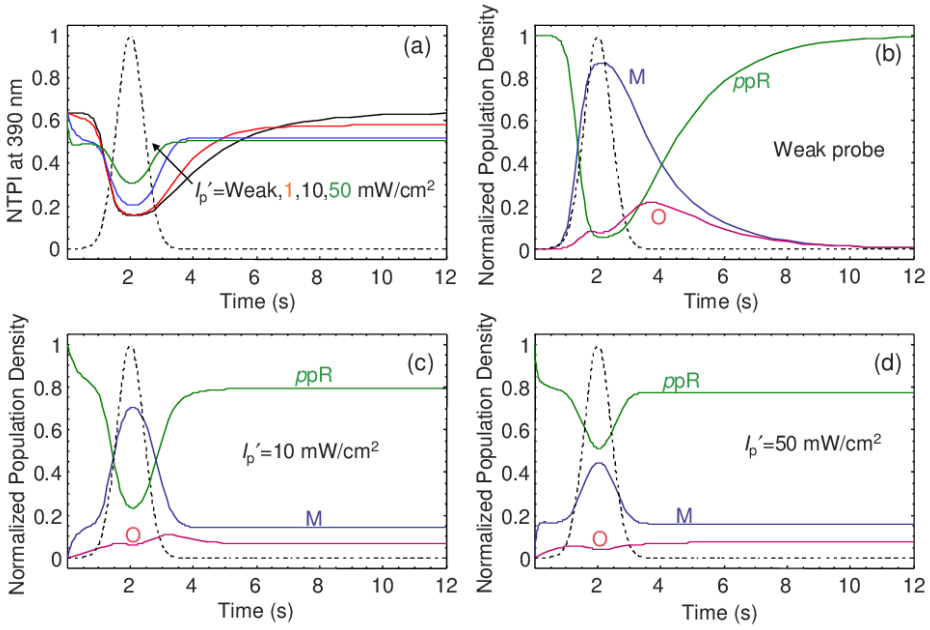

Fig. 2. (a) Variation of NTPI at 390 nm for normalized input pulse at 498 nm (dashed line) with time for different I_p' values in WT-*p*pR, and variation of the normalized population density of *p*pR, M and O states for normalized input pulse at 498 nm (dashed line) with time for (b) Weak probe intensity, (c) I_p' = 10 mW/cm^2 and (d) I_p' = 50 mW/cm^2, with Δt = 1 s, I_{m0}' = 50 mW/cm^2 for C = 47.02 μM.

An intense probe beam affects the population dynamics of intermediates by exciting the *p*pR molecules in the initial ground state even in the absence of the pump pulse, as shown in Figs. 2(b)–2(d). As I_p' increases, the equilibrium population (population in the presence of intense cw probe beam only) of initial *p*pR state decreases and the equilibrium populations of longer-lived M and O states increase. The increased absorption of probe beam at 390 nm by M excited-state decreases its transmission in the absence of the pump pulse, as shown in Fig. 2(a). The population of M-state molecules excited by pulsed pump beam also decreases with increase in I_p', as these molecules relax fast into the initial *p*pR state. This is due to increase in effective rate constant of M intermediate by intense probe beam ($k_{M\text{-}Eff} = k_M + I_p\sigma_{Mp}$), as shown in Figs. 2(b)–2(d). This reduces the switching contrast and switching time as well. For instance, for a very weak probe beam, the NTPI is modulated by 48.15% with switch 'off' and 'on' time of ~1.5 s and 9 s, respectively, while for I_p' = 50 mW/cm^2, the NTPI is modulated by 19.65% with switch 'off' and 'on' time of 1.4 s and 2 s, respectively. As expected, the decrease in effective lifetime of M intermediate state also results in increase in symmetry of the switched probe beam, as the pulse width becomes greater and conforms to the steady-state condition.

Hence, as is well known, the transmission of a weak probe beam, corresponding to the wavelength at which γ is high, exhibits negative switching. Our analysis shows that the switching time in this case, can be decreased by increasing I_p', provided the probe beam is also absorbed by the initial state. The symmetry of switched probe beam in this case also increases with decrease in switching contrast.

In general, pump and probe beams are considered at the peak absorption wavelength of ground and excited states, respectively. For analyzing the effect of the spectral response, we consider pump and probe beams at other wavelengths, i.e. with probe beams at 498 nm and 390 nm, respectively, and a pulsed pump beam at 390 nm. Figure 3(a) shows the variation of NTPI at 498 nm with time due to pump pulse excitation at 390 nm for different I_p' values. Interestingly, in this case, the switching characteristics can be inverted from 'positive' to

#160815 - $15.00 USD Received 3 Jan 2012; revised 8 Mar 2012; accepted 20 Mar 2012; published 6 Apr 2012

'negative' by increasing I_p'. It is clear from Fig. 3(a) that there is an optimum value of I_p' for which maximum switching contrast can be obtained. The calculated value of maximum switching contrast in this case is 54.16%, for an optimum I_p' = 23 mW/cm^2. For a weak probe beam at 498 nm, the initial NTPI in the absence of pump pulse is low, due to high absorption by initial *p*pR state only. In this case, as the modulating pulse appears, the NTPI exhibits 'positive switching' due to decreased absorption of probe beam by depleted population of initial *p*pR state, after absorption of pump at 390 nm. Increasing I_p' at 498 nm decreases the population of initial *p*pR state, due to its excitation to longer-lived M and O intermediate states that leads to increase in NTPI in the absence of the pump pulse. The pump pulse excitation at 390 nm in this case, results in photo-induced relaxation of populated M-state to *p*pR state that leads to 'negative switching'.

Considering both the pump and probe beams at 390 nm in WT-*p*pR, the switching characteristics again get inverted from 'negative' to 'positive', on increasing I_p'. For a particular I_p', the NTPI remains unmodulated by pump pulse i.e. the material appears to be optically linear for a particular value of I_p'. The NTPI at 390 nm considering weak probe beam transmission, exhibits 'negative switching' due to increased absorption of probe beam by populated M-state, Fig. 3(b). Increase in I_p' in this case, decreases the NTPI in the absence of pump pulse due to increased absorption of probe beam by populated M-state. The excitation of sample with pump pulse at 390 nm results in photoinduced relaxation of M-state to initial *p*pR state that leads to decreased absorption of probe beam i.e. 'positive switching', Fig. 3(b).

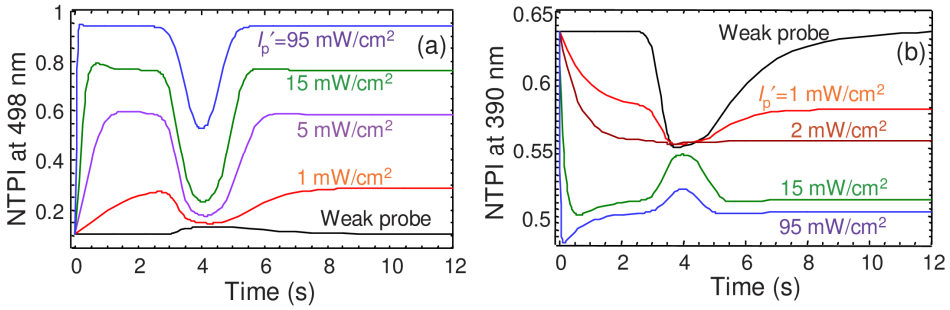

Fig. 3. Variation of NTPI at (a) 498 nm and (b) 390 nm, for input pulse at 390 nm with time for different I_p' values in WT-*p*pR, with Δt = 1 s, I_{m0}' = 50 mW/cm^2 for C = 47.02 μM.

All-optical switching characteristics for O-state dynamics have also been studied in WT-*p*pR. The absorption spectra of different intermediates show that O-state exhibits maximum absorption at 560 nm, whereas other states have very low absorption at this wavelength [39–43]. The switching characteristics for this case considering weak probe transmission at 560 nm, (Fig. 4(a)), shows 'negative switching', qualitatively similar to 390 nm case, Fig. 2(a). There is an optimum value of concentration (120 μM), for which maximum switching contrast (35.28%) of the NTPI can be achieved. The optimum value of concentration decreases with increase in I_{m0}' [18]. For peak pump intensities of 5 and 10 mW/cm^2, the optimum values of concentration are 139 μM and 129 μM, respectively, with 27.16% and 32.45% maximum switching contrast.

Figure 4(a) shows the effect of variation of I_p' on NTPI at 560 nm with I_{m0}' = 50 mW/cm^2. As I_p' increases, the switching contrast of NTPI at 560 nm and switching time decrease. At a particular I_p' value, the switching contrast becomes negligible. Further increase in I_p' results in 'positive switching'. This variation in the nature of switching characteristics can be explained considering intensity-induced population changes of different intermediates as shown in Figs. 4(b)–4(d).

#160815 - $15.00 USD Received 3 Jan 2012; revised 8 Mar 2012; accepted 20 Mar 2012; published 6 Apr 2012

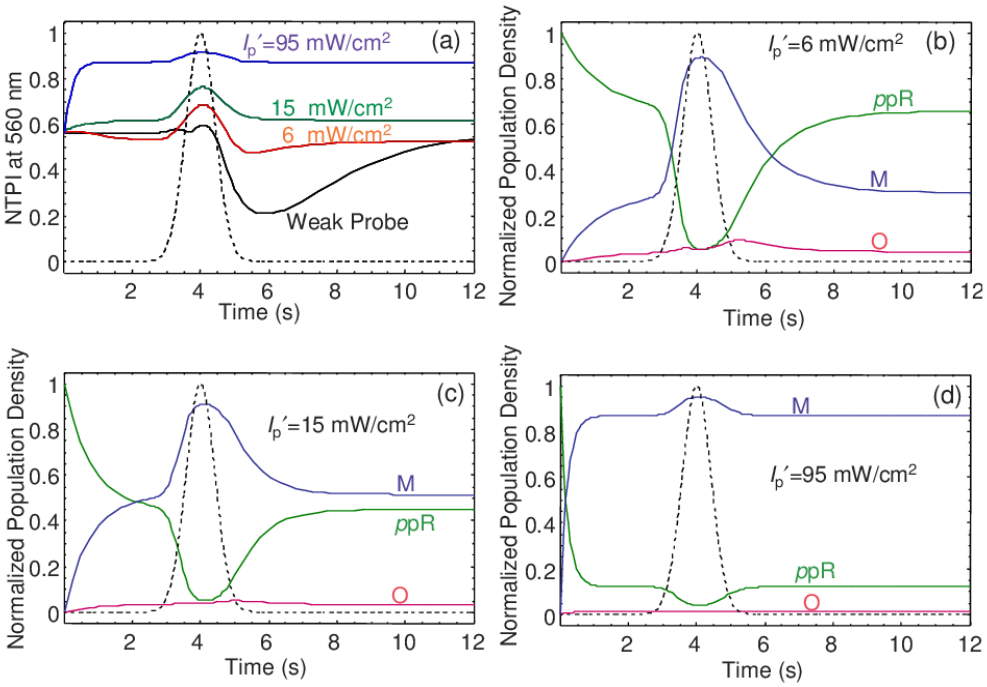

Fig. 4. (a) Variation of NTPI at 560 nm for normalized input pulse at 498 nm (dashed line) with time for different I_p' values in WT-*p*pR, and variation of the normalized population density of *p*pR, M and O states for normalized input pulse at 498 nm (dashed line) with time for (b) I_p' = 6 mW/cm^2, (c) I_p' = 15 mW/cm^2 and (d) I_p' = 95 mW/cm^2, for Δt = 1 s, I_{m0}' = 50 mW/cm^2, C = 120 μM.

As I_p' at 560 nm increases, the equilibrium population of the initial *p*pR state decreases due to its excitation. The longer-lived M-state does not exhibit any absorption at 560 nm [39,40]. Hence, the equilibrium population of M-state increases with increase in I_p'. The O-state molecules are absorbed by the intense probe beam. Thus, its equilibrium population decreases and becomes very low, as shown in Figs. 4(b)–4(d). For lower I_p' values, as the pump pulse excites the sample, initially the NTPI increases due to decreased absorption by depleted *p*pR state and after some time, it decreases due to increased absorption of probe beam by O-state molecules relaxed from M-state, as shown in Figs. 4(a) and 4(b). Further increase in I_p' results in more increase in equilibrium population of M-state and decrease in equilibrium population of *p*pR state. The excitation of the *p*pR sample by pump pulse in this case, decreases the population of initial *p*pR state and increases the population of M-state, whereas it does not cause any significant change in the population of O-state, as shown in Fig. 4(c). Thus, the NTPI in this case increases from its equilibrium value due to smaller absorption of the probe beam by depleted *p*pR state, as shown in Figs. 4(a) and 4(c) at I_p' = 15 mW/cm^2. Very high I_p' (95 mW/cm^2) results in large decrement in population of the initial *p*pR state that finally results in increase in NTPI in the absence of pump pulse and decrease in switching contrast, as shown in Figs. 4(a) and 4(d). There is again an optimum value of I_p' (15 mW/cm^2) for which maximum modulation occurs, as in Fig. 3(a).

In general, as is well known, the longer-lived probed state with high γ values results in 'negative switching'. The present analysis shows that if the probed state has a longer-lived earlier intermediate state that has no absorption at both probe and pump wavelengths, the switching characteristics can be inverted from 'negative' to 'positive' by increasing I_p'. The switching contrast expectedly becomes very low for higher I_p' values.

#160815 - $15.00 USD Received 3 Jan 2012; revised 8 Mar 2012; accepted 20 Mar 2012; published 6 Apr 2012

Figure 5(a) shows the variation of NTPI at 498 nm due to pump pulse excitation at 560 nm, for different I_p' values in WT-*p*pR. Considering weak probe beam transmission, NTPI exhibits 'positive switching' due to decreased absorption of probe beam by depleted population of *p*pR state by pump pulse excitation. Increase in I_p' results in increase in NTPI in the absence of pump pulse due to decreased absorption of probe beam by depleted *p*pR state. The switching contrast in this case also decreases with increase in I_p'. Figure 5(b) shows the variation of NTPI at 560 nm with time, due to pump pulse excitation at 560 nm for different I_p' values. The temporal variation of NTPI at 560 nm due to pump pulse excitation at 560 nm (Fig. 5(b)), is similar to temporal variation of NTPI at 560 nm due to pump pulse excitation at 498 nm (Fig. 4(a)), due to major role of *p*pR and O state populations in both the cases.

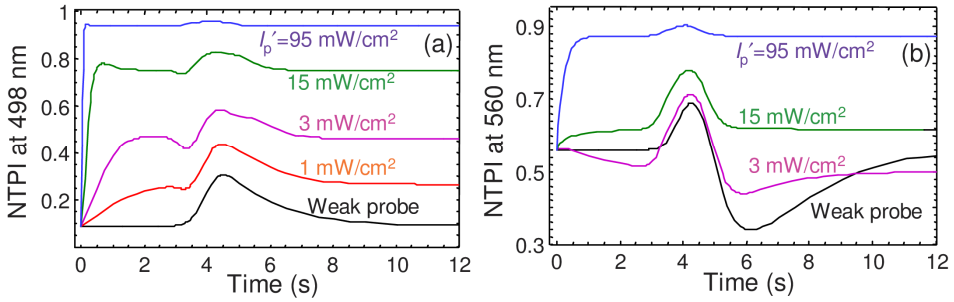

Fig. 5. Variation of NTPI at (a) 498 nm and (b) 560 nm, for input pulse at 560 nm with time for different I_p' values in WT-*p*pR, with Δt = 1 s, I_{m0}' = 50 mW/cm² for C = 120 μM.

3.2 F86D/L40T-ppR Mutant

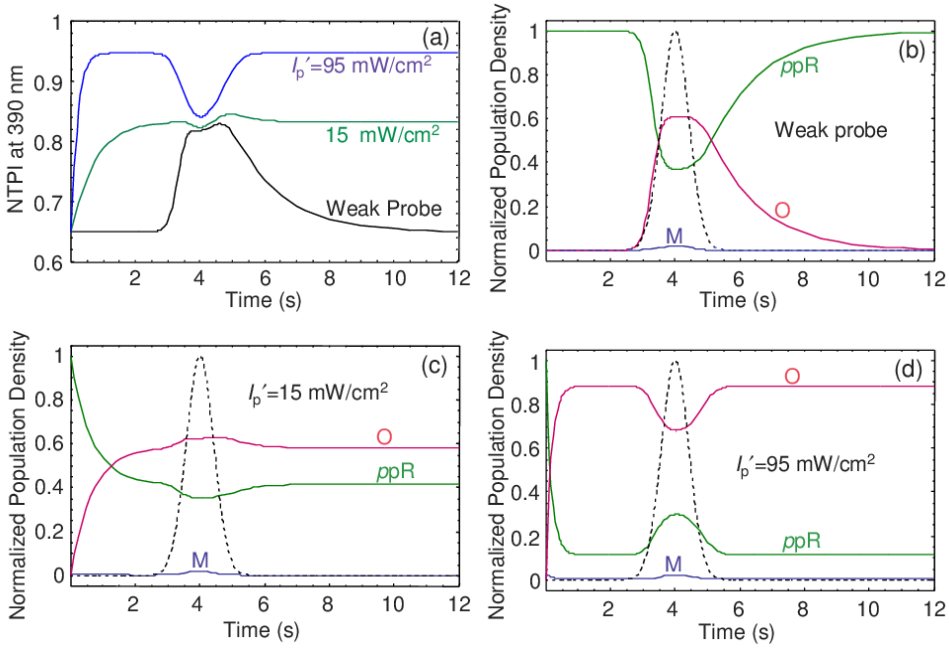

Fig. 6. (a) Variation of NTPI at 390 nm with time for different I_p' values in F86D/L40T-*p*pR at pH = 5, and variation of the normalized population density of *p*pR, M and O states for normalized input pulse at 498 nm (dashed line) with time for (b) Weak probe intensity, (c) I_p' = 15 mW/cm² and (d) I_p' = 95 mW/cm², with Δt = 1 s, I_{m0}' = 50 mW/cm² for C = 44.8 μM.

#160815 - $15.00 USD Received 3 Jan 2012; revised 8 Mar 2012; accepted 20 Mar 2012; published 6 Apr 2012

F86D/L40T-*p*pR mutant exhibits longer-lived O-intermediate and shorter lived M intermediate state. Figure 6(a) shows the variation in the NTPI at 390 nm with time for different I_p' values for F86D/L40T-*p*pR mutant at pH = 5 with concentration of 44.8 μM, i.e., optimum concentration for maximum switching contrast for weak probe beam. It is clear from Fig. 6(a) that by increasing I_p' at 390 nm, the switching characteristics get inverted with decrease in total switching time and increase in symmetry.

The transmission of a weak probe beam exhibits 'positive switching', as shown in Fig. 6(a). The population dynamics for a weak probe beam is shown in Fig. 6(b). The population of M-state in this case is very small due to its very short lifetime. Hence, the NTPI at 390 nm depends upon the small absorption by the initial *p*pR state. In this case, the NTPI increases due to lower absorption of the probe by the less populated shorter lifetime M-state and the depleted initial *p*pR state [30,44].

The intense probe beam increases the equilibrium population of O-state by exciting *p*pR molecules, as shown in Figs. 6(b) and 6(c). This is due to short lifetime of M intermediate state and no absorption of longer-lived O-state at 390 nm [39,40]. The depletion in the population of the initial *p*pR state with no significant variation in population of the shorter lived M-state increases the NTPI at 390 nm in the absence of pump pulse. At moderate I_p' (~15 mW/cm^2), the equilibrium population of *p*pR state is smaller than O-state and satisfies the condition: $N_R(I_p)\sigma_R \approx N_O(I_p)\sigma_O$. The excitation of sample by pump pulse in this case causes no significant variation in the populations of *p*pR and O intermediate states. This results in switching characteristics nearly unmodulated by pump pulse. At high I_p', the equilibrium population of O-state becomes very large and the equilibrium population of *p*pR state becomes very small, as shown in Fig. 6(d). In this case, the excitation of *p*pR sample by pulsed pump beam at 498 nm results in increase in population of initial *p*pR state due to photoinduced relaxation of highly populated *p*pR$_O$ state molecules into less populated initial state. This decreases the NTPI at 390 nm due to increased absorption of the probe beam by the initial state and leads to 'negative switching'. For instance, considering a weak probe, the NTPI is modulated by 17.97%, with the switch on-time of 2 s and the switch-off time of 7 s. At I_p' = 15 mW/cm^2, the switching contrast becomes negligible. At I_p' = 95 mW/cm^2, inverted switching characteristics are obtained with 10.55% contrast, with off and on-time of ~1.5 s and 2 s, respectively. The switching time decreases and symmetry of switched probe beam increases with increase in I_p' due to increase in the effective rate constant of O-state for photoinduced transformation.

Hence, in a molecular system, if the probed state has a shorter lifetime and γ is higher at probe wavelength, then the NTPI exhibits 'positive switching' provided the initial state exhibits substantial absorption at probe wavelength. The switching characteristics in this case, can be inverted by using intense probe beam provided a longer-lived state comes after the probed state and which has no absorption at probe wavelength. The switching time in this case also decreases with increase in symmetry of switching characteristics.

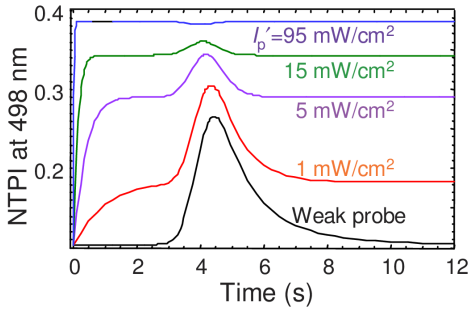

Fig. 7. Variation of NTPI at 498 nm for input pulse at 390 nm with time for different I_p' values in F86D/L40T-*p*pR, with Δt = 1 s, I_{m0}' = 50 mW/cm^2 for C = 47.02 μM.

#160815 - $15.00 USD Received 3 Jan 2012; revised 8 Mar 2012; accepted 20 Mar 2012; published 6 Apr 2012

Considering the weak probe beam transmission and pump pulse excitation at 390 nm, the NTPI at 498 nm in F86D/L40T-*p*pR also exhibits 'positive switching' with higher contrast in comparison to WT-*p*pR case, as shown in Figs. 3(a) and 7. This is due to shorter lifetime of M-state in comparison to O-state having no absorption at 390 nm, in F86D/L40T-*p*pR. This leads to comparatively higher utilization of 390 nm pump pulse in F86D/L40T-*p*pR for exciting the initial state in comparison to photo-induced back relaxation of M-state to initial state. The 'positive switching' contrast in this case decreases with increase in I_p' similar to the variation shown in Fig. 5(a). At very high I_p' values, the switching characteristics invert (negative switching) with low switching contrast, due to very small population of shorter lived M-state. The variation in NTPI at 390 nm due to pump pulse excitation at 390 nm in F86D/L40T-*p*pR is similar to the earlier case, Fig. 7.

The switching characteristics can be inverted from 'positive' to 'negative' by increasing I_p' at 498 nm with pump pulse at 560 nm, Fig. 8(a). Considering the weak probe beam transmission, the NTPI at 498 nm due to pump pulse excitation at 560 nm, exhibits 'positive switching' with very low switching contrast, Fig. 8(a). Higher I_p' in this case results in 'negative switching' due to increased absorption of probe beam by longer-lived O-state, which is highly populated due to intense probe beam and pump pulse excitation. In this case, similar to WT*p*pR case described by Fig. 3(a) and 4(a), there is an optimum value of $I_p' = 15$ mW/cm^2 (see Fig. 8(a)) for which maximum switching contrast (18.3%) can be achieved.

All-optical switching considering both pump and probe beams at 560 nm, respectively, have also been studied. The NTPI at 560 nm considering weak I_p', exhibits 'negative switching' due to long lifetime of O-state, Fig. 8(b). Increase in I_p' in this case leads to increase in population of O-state that results in decrease in the NTPI in the absence of pump pulse. The excitation of sample by pump pulse in this situation, switches the highly populated O-state molecules to initial state, which leads to decreased absorption of probe beam i.e. 'positive switching', Fig. 8(b).

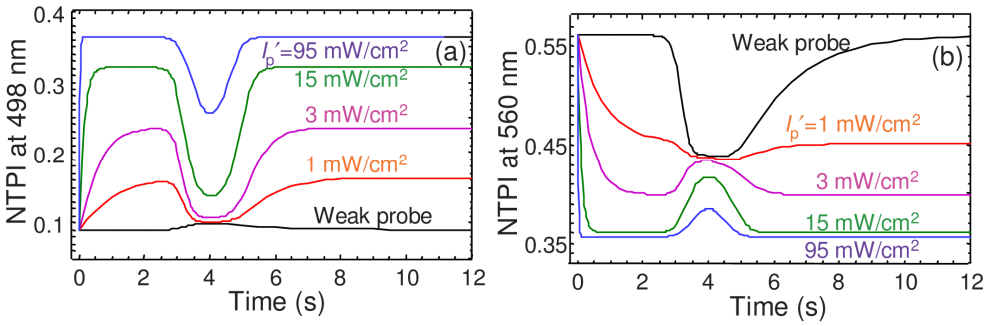

Fig. 8. Variation of NTPI at (a) 498 nm and (b) 560 nm, for input pulse at 560 nm with time for different I_p' values in F86D/L40T-*p*pR, with $\Delta t = 1$ s, $I_{m0}' = 50$ mW/cm^2 for $C = 120$ μM.

3.3 F86D-ppR Mutant

In this mutant, the M-state lifetime is less than that in WT-*p*pR and higher than that in F86D/L40T-*p*pR and the O-state lifetime is more than that in WT-*p*pR and less than that in F86D/L40T-*p*pR [45]. Figure 9(a) shows the variation in the NTPI at 390 nm with time for different I_p' values for F86D-*p*pR mutant at pH = 5 with concentration of 44.8 μM. It is clear from the figure that an increase in I_p' at 390 nm results in increase in NTPI in the absence of pump pulse, i.e., 'negative switching' with increase in switching contrast. Switching characteristics in this case also become symmetric with decrease in switching time at higher I_p'.

Considering the weak probe case, the NTPI initially decreases as pump pulse excites the sample and after some time increases above the linear transmission value before saturating to

#160815 - $15.00 USD Received 3 Jan 2012; revised 8 Mar 2012; accepted 20 Mar 2012; published 6 Apr 2012

its linear value again, Fig. 9(a). The population dynamics of the intermediates in this mutant is shown in Fig. 9(b). As the pump pulse excites the *p*pR molecules, initially the populations of M and O states increase, which result in decrease in NTPI. After some time the molecules of relatively shorter lived M-state relax into the longer lived O-state, which has no absorption at 390 nm that results in increase in NTPI. Finally, relaxation of O-state molecules to initial state leads to saturation of NTPI to its linear value.

Increasing I_p' results in increase in the equilibrium population of O-state and decrease in the equilibrium population of initial *p*pR state, as shown in Figs. 9(c) and 9(d). This is due to no absorption by longer lived O-state at 390 nm [39,40], which results in increase in NTPI in the absence of the pump pulse. Increase in the equilibrium population of M-state is very low due to its photo-induced relaxation to initial state by absorbing the intense probe beam at 390 nm. At higher I_p', the equilibrium population of O-state becomes very large in comparison to the population of the initial *p*pR state, as shown in Fig. 9(d). In this case, the excitation of *p*pR sample by pulsed pump beam at 498 nm results in increase in population of both the M-state due to its long lifetime, and the initial *p*pR state due to photoinduced relaxation of highly populated O-state molecules into the less populated initial state. This results in higher absorption of the probe beam i.e. 'negative switching'. In contrast to earlier cases, in this case, the switching contrast increases with increase in its intensity.

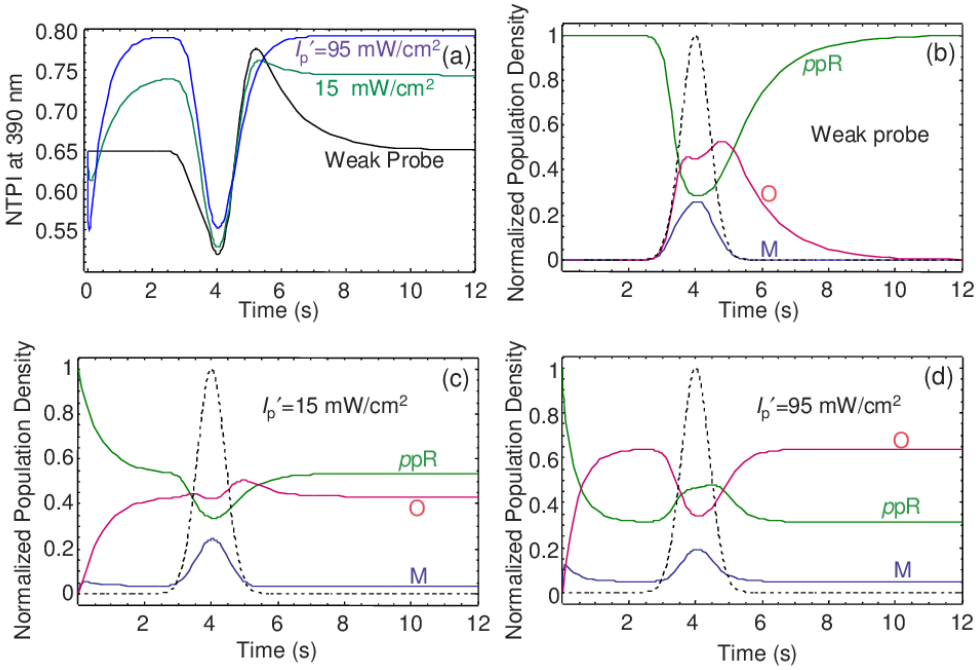

Fig. 9. (a) Variation of NTPI at 390 nm with time for different I_p' values in F86D-*p*pR at pH = 5, and variation of the normalized population density of *p*pR, M and O states for normalized input pulse at 498 nm (dashed line) with time for (b) Weak probe intensity, (c) I_p' = 15 mW/cm^2 and (d) I_p' = 95 mW/cm^2, with Δt = 1 s, I_{m0}' = 50 mW/cm^2 for C = 44.8 μM.

As shown in Fig. 10, the nature of temporal variation of NTPI at 498 nm due to pump pulse excitation at 390 nm can be inverted, by increasing I_p' at 498 nm. The contrast for 'positive' and 'negative' switching at lower and higher I_p' is comparable in F86D-*p*pR, due to moderate lifetime of M-state in this mutant. Switching contrast for 'positive switching' of NTPI at 390 nm in F86D-*p*pR due pump pulse excitation at 390 nm, also decreases with increase in I_p', similar to Fig. 7.

#160815 - $15.00 USD Received 3 Jan 2012; revised 8 Mar 2012; accepted 20 Mar 2012; published 6 Apr 2012

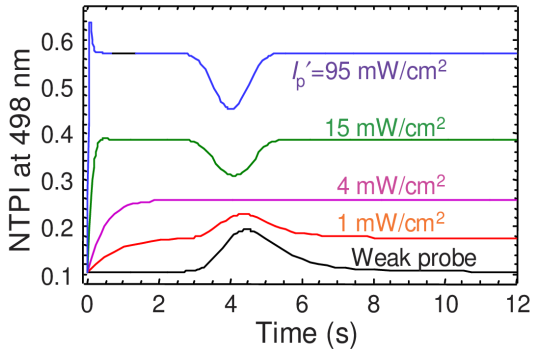

Fig. 10. Variation of NTPI at 498 nm and for input pulse at 390 nm with time for different I_p' values in F86D-*p*pR, with Δt = 1 s, I_{m0}' = 50 mW/cm^2 for C = 47.02 μM.

Figure 11 shows the effect of variation of I_p' at 498 nm for pump pulse at 560 nm in F86D-*p*pR. As in case of WT-*p*pR (Fig. 5(a)), and F98D/L40T-*p*pR (Fig. 8(a)), F86D-*p*pR also exhibits 'positive switching' for weak probe beam transmission. Increase in I_p' results in 'negative switching' as for F86D/L40T-*p*pR, Fig. 8(a). Interestingly, further increase in I_p' results in 'positive switching', Fig. 11.

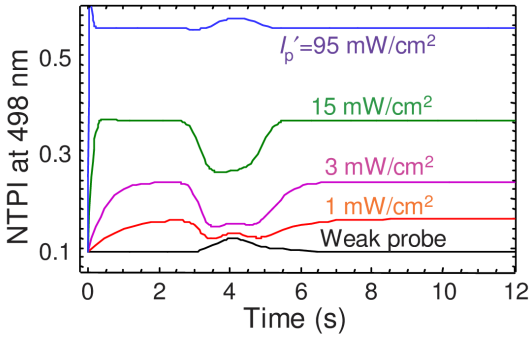

Fig. 11. Variation of NTPI at 498 nm for input pulse at 560 nm with time for different I_p' values in F86D-*p*pR, with Δt = 1 s, I_{m0}' = 50 mW/cm^2 for C = 120 μM.

Since the kinetic and spectral properties of *p*pR can be tailored by various methods, the switching characteristics can be optimized to increase the contrast and obtain faster response time [38–50]. The effect of I_p' on switching characteristics at a given wavelength would depend on the rate constants of intermediates and overlap of spectra of different states at pump and probe wavelengths, respectively. The general inferences are valid for a wide class of photosensitive proteins that exhibit a photocycle such as archael rhodopsins, bacteriorhodopsin [24,28–30], halorhodopsin [51], proteorhodopsin [52] etc., photoactive yellow protein [53], LOV2 [54], phototropin etc. The present analysis is useful to draw general inferences applicable to these photochromic molecular systems. In these systems, relaxation rates for initial intermediate states (e.g. K, KL, L of *p*pR) of the photocycle are generally very large. It is normally assumed that these rates are so large that the population densities of these states are very small for low energy pump pulse excitations and can be neglected [30]. Under these assumptions, a three-level model adequately accounts for the photoresponse as shown in Figs. 12(a) and 12(b). Considering a photochromic molecule with a schematic level diagram as shown in Fig. 12(a), the general inferences have been summarized in Table 2. This would be useful to analyze a wide range of materials that may exhibit such characteristics or would help in tuning the characteristics to meet the desired requirements shown.

#160815 - $15.00 USD Received 3 Jan 2012; revised 8 Mar 2012; accepted 20 Mar 2012; published 6 Apr 2012

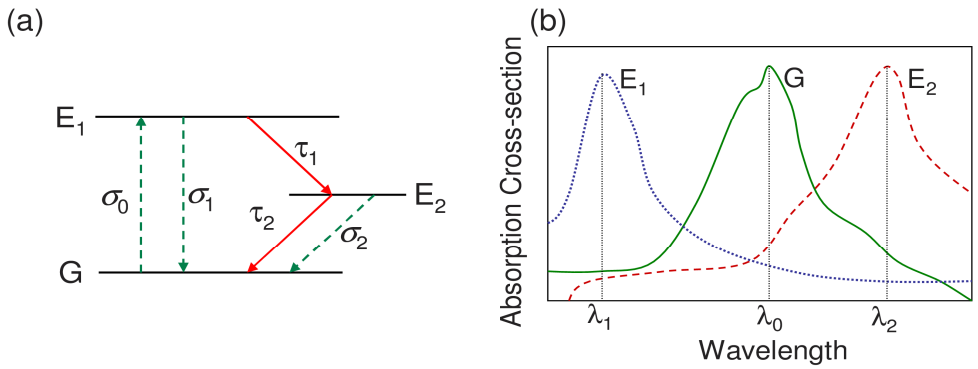

Fig. 12. (a) Simplified level diagram having three states; G: Ground State, E_1 and E2: Intermediate States. (b) The arbitrary absorption spectra of all the three states.

The detailed analysis also provides important insights in controlling the population dynamics in different intermediate states by I_p'. By simply controlling I_p', important switching parameters such as, the response time, contrast and profile can be controlled. The general inferences that have been drawn from the analysis of *p*pR are applicable to a wide variety of photochromic systems. Photosensitive proteins in particular provide interesting possibilities to control the nonlinear optical response due to (i) more number of intermediate states, (ii) large overlap of respective absorption spectra, (iii) sophisticated control of spectral and kinetic response over a wide range through nano-biotechnology and (iv) low-power operation.

Since, a switch is the basic unit of information processing systems, the present analysis may be useful in the design of various all-optical devices based on nonlinear absorption such as logic gates, spatial light modulators, bistable devices. Although one would be tempted to think that proteins would not meet the stringent requirements of thermal and photo-stability for any practical applications, bR and *p*pR exhibit remarkable stability. It has been experimentally demonstrated that bR can undergo more than 10^6 number of switching cycles without getting denatured [24]. The reversibility of bR is astonishingly high. Leophyl-dried purple membrane preparation has no storage limit. bR can retain its folded native structure up to temperatures as high as 140 ^{0}C, incorporated in multilayer structures of self-assembled ordered films [55,56]. These exceptional properties are attributed to its survival in extremely harsh conditions, having been optimized over centuries of evolution and possessing a 2-D crystalline structure. bR and ppR have also been shown to be stable at 80^{0}C in liquid form [24,57]. bR stability surpasses that of other synthetic organic molecules. Our experiments on all-optical switching with both bR and *p*pR reported earlier at room temperature show excellent stability [32,44].

The photocycle of both bR and *p*pR exhibit short and long-lifetime intermediates. The early photoreaction on absorption of a photon is extremely fast < ps, whereas the later states thermally relax ~ms-s. The present analysis would be applicable for faster switching using the early intermediates. We have already shown that exposing the molecules with high repetition rate pump pulses and an additional bias beam to truncate the photocycle, can lead to switching ~μs [31,41]. In addition, ultrafast absorption changes observed in bR may lead ultrafast switching [58]. Moreover, integration of these ultrasensitive photochromic proteins with nanostructures also opens up exciting possibilities for faster switching [59,60].

Switching response of a photosensitive material basically depends on its spectral or kinetic properties [13,18–20,30,32,41–44,52]. Different applications require different material properties and hence different samples. By controlling I_p', the population dynamics and material response can be controlled to achieve different operations without changing the sample.

#160815 - $15.00 USD Received 3 Jan 2012; revised 8 Mar 2012; accepted 20 Mar 2012; published 6 Apr 2012

(A) $\tau_1>\tau_2$	**At λ_m: $\gamma_1<1$, $\sigma1 = 0$ At λ_p: $\gamma_1>1$, $\sigma_2 = 0$ At λ_2: $\sigma_1 = 0$**		**At λ_m: $\gamma_1>1$, $\sigma_2 = 0$ At λ_p: $\gamma_1<1$, $\sigma1 = 0$ At λ_2: $\sigma_1 = 0$**		**At λ_m: $\gamma_2<1$, $\sigma_1 = 0$ At λ_p: $\gamma_2>1$, $\sigma_1 = 0$ At λ_1: $\sigma_2 = 0$**		**At λ_m: $\gamma_2>1$, $\sigma_1 = 0$ At λ_p: $\gamma_2<1$, $\sigma_1 = 0$ At λ_1: $\sigma_2 = 0$**		**At $\lambda_m = \lambda_p$: $\gamma_1>1$, $\sigma_2 = 0$ At λ_0: $\sigma_1 = 0$ At λ_2: $\sigma_1 = 0$**		**At $\lambda_m = \lambda_p$: $\gamma_2>1$, $\sigma_1 = 0$ At λ_1: $\sigma_2 = 0$**	
Relative Effect	Weak Probe	Strong Probe	Weak Probe	Strong Probe	Weak Probe	Strong Probe	Weak Probe	Strong Probe	Weak Probe	Strong Probe	Weak Probe	Strong Probe
Switching Contrast	High	Low	Low	High	High	Low	High	Low	High	Low	High	Low
Phase relation of pump/probe	-ve	-ve	+ ve	-ve	-ve	+ ve	-ve	-ve	-ve	+ ve	+ ve -ve	+ ve
(B) $\tau_2>>\tau_1$												
Relative Effect	Weak Probe	Strong Probe	Weak Probe	Strong Probe	Weak Probe	Strong Probe	Weak Probe	Strong Probe	Weak Probe	Strong Probe	Weak Probe	Strong Probe
Switching Contrast	High	Low	High	Low	High	Low	Low	High	High	Low	High	Low
Phase relation of pump/probe	+ ve	-ve	+ ve	-ve (small contrast)	-ve	-ve	+ ve	-ve	+ ve	+ ve	-ve	+ ve
(C) $\tau_2>\tau_1$												
Relative Effect	Weak Probe	Strong Probe	Weak Probe	Strong Probe	Weak Probe	Strong Probe	Weak Probe	Strong Probe	Weak Probe	Strong Probe	Weak Probe	Strong Probe
Switching Contrast	Low	High	Comparable		High	Low	Low	High	High	Low	Comparable	
Phase relation of pump/probe	-ve + ve	-ve	+ ve	-ve	-ve	-ve	+ ve	-ve then + ve	+ ve	-ve (less contrast)	-ve	+ ve
The parameters, $\gamma_1 = \sigma_1/\sigma_0$ and $\gamma_2 = \sigma_2/\sigma_0$, where σ_0, σ_1 and σ_2 are the absorption cross-section values of G, E_1 and E_2 states, respectively. Switching time decreases and symmetry of switched probe beam increases with increase in probe intensity for all cases.												

Table 2. Relative Effect of Probe Intensity on Switching Characteristics at Different Spectral and Kinetic Conditions of Molecular System Represented in Fig. 12

#160815 - $15.00 USD
Received 3 Jan 2012; revised 8 Mar 2012; accepted 20 Mar 2012; published 6 Apr 2012

For instance, for $\gamma<1$ at probe wavelength, 'positive switching' is observed that can be used to design AND and OR logic gates. For $\gamma>1$ at probe wavelength, 'negative switching' is observed that can be used to design NOT, NAND and NOR logic gates [29,30]. As shown in the present study, both 'positive' and 'negative' switching can be achieved in the same sample, by only controlling the probe intensity. Hence, all-optical NOT, NAND, NOR, AND and OR logic operations can be realized using the same sample.

Recently, controllable ultraslow light has been demonstrated in a thin bR film (~0.091 mm/s) based on coherent population oscillations, at room temperature [61]. The present analysis would also be potentially useful in probe intensity controlled all-optical switching with controllable delay, over a wide range, using the same sample.

4. Conclusion

We have theoretically analyzed the effect of I_p' on all-optical switching based on nonlinear absorption, using the pump-probe configuration. General inferences applicable to a wide range of photochromic molecules have been drawn by conducting a detailed analysis of switching in *p*pR protein and its mutants that exhibit a complex photocycle. It has been shown that by controlling I_p', the switching characteristics can be inverted, switching time can be reduced and the profile of the switched probe beam and the switching contrast can be controlled. For some cases, the switching contrast can also be maximized by optimizing I_p'. Under certain conditions, increase in I_p' also leads to increase in switching contrast. For a given I_p' and pump-probe wavelength combination, at particular spectral and kinetic conditions, the nonlinear optical material appears linear. The switching characteristics can hence be modified by varying I_p' instead of using mutants with different rate constants, to design a variety of nonlinear absorption based all-optical devices.

Acknowledgments

PS thanks Council of Scientific and Industrial Research, India, for financial support, and Director, CSIR-NPL, New Delhi, and Dr. H.C. Kandpal, for their support and encouragement.

#160815 - $15.00 USD Received 3 Jan 2012; revised 8 Mar 2012; accepted 20 Mar 2012; published 6 Apr 2012